

Electron, optical, and magneto-optical properties of semimetallic and uranium-containing ferromagnets

E. T. Kulatov

Institute of General Physics, USSR Academy of Sciences

S. V. Khalilov

Kurchatov Institute of Atomic Energy

(Submitted 4 June 1990)

Zh. Eksp. Teor. Fiz. **98**, 1778–1789 (November 1990)

The formalism of the local-spin-density functional, with allowance for all the relativistic terms, is used to calculate the electron, optical, and magneto-optical spectra of a number of semimetallic ferromagnets and of uranium chalcogenides. It is shown that the gain of the magneto-optic Kerr effect in semimetallic ferromagnets is closely connected with spin-orbit and exchange splitting. At the same time, the anomalies of the conductivity tensor in ordinary ferromagnets, at energies of the order of the spin-orbit splitting, are due to the peculiarities of the band structure near the Fermi level.

INTRODUCTION

Following the experimental observation¹ of the giant polar magneto-optic Kerr effect (MOKE) in the intermetallic compound PtMnSb, theoretical interest in the study of the electronic and optical properties of analogous compounds has greatly increased. Calculation² of the electronic structure of NiMnSb has pointed to the existence of a new class of substances, called half-metallic ferromagnets (HMF). The reason for this name is that in NiMnSb the Fermi level in the spin subband of the minority-spin electrons (SSI) is located inside the energy gap, while in the spin subband of the majority-spin electrons (SSA) crosses the energy bands. This means, in particular, that Fermi electrons have 100% spin polarization. Later band calculations³ have shown that NiUSn is also an HMF. The cause of the band gap in HMF is the lowering of the symmetry on going from the usual Heusler alloys with structure formula T_2MnZ (T is a $3d$ metal, Z is Sb or Sn) to HMF with non-centrosymmetric TMnZ structure. From the standpoint of applications the investigation of such compounds is justified by the search for substances having a sufficiently high MOKE, in view of the known need for developing a technology for magneto-optic recording and storage of information.

The much higher MOKE in PbMnSb compared with NiMnSb is attributed in Ref. 1 to the different positions of the Fermi energy E_F in these compounds relative to the energy-gap bottom in SSI and to the different values of the spin-orbit interaction (SOI). It was shown in Ref. 4, however, that the location of E_F relative to the gap is extremely sensitive to the form of the local exchange-correlation potential and cannot be determined with required accuracy in a local approximation. An attempt to attribute the large MOKE in PtMnSb to plasma resonance was undertaken in Ref. 5. Anomalous MOKE was predicted on the basis of calculations for NiUSn.⁶

To cast light on the causes of the anomalously large MOKE in HMF we have investigated the effects of SOI on the electronic structure, and also performed fully relativistic computations of the optical and magneto-optic spectra of a number of HMF. One of the purposes of these calculations was to clarify the role played by the semiconductor gap in

SPI of a half-metal ferromagnet in the onset of the MOKE. For comparison, in addition to calculating the conductivity tensor $\sigma_{\alpha\beta}(\omega)$ for HMF, the band spectrum and the conductivity tensor were calculated for the chalcogenide US, in which the SOI and the exchange-interaction effects are of the same order as, for example, in NiUSn, but there is no energy gap in the spectrum.

1. CALCULATION METHOD AND BASIC EQUATIONS

To carry out scalar-relativistic spin-polarization calculations of the band structures of NiMnSb, PtMnSb, NiUSn, and US in the formalism of the local-spin-density functional (the von Barth–Hedin approximation), we used the FTIR method⁷ with allowance for combined correction terms in MgAgAs and NaCl structures. To obtain self-consistent potentials we used 88 k-points in 1/48 irreducible part of the Brillouin zone (IPBZ). We introduced into MgAgAs structure one empty sphere to increase the degree of packing. All the calculations were performed for experimental equilibrium lattice parameters. The SOI effects were included in the band calculations by the Kohn–Foldy–Vouthuisen equation,⁸ which corresponds in fact to the Russell–Saunders LS scheme. The single-particle spectrum obtained in this manner is used to calculate the conductivity tensor in accordance with the Kubo formula for linear-response functions.⁹

The matrix elements of the dipole transitions were calculated directly with the aid of the wave functions using the scheme described in Ref. 10. It is known that the general form of the conductivity tensor is determined by the magnetic space group of the crystal and depends thus on the orientation of the magnetization \mathbf{M} . For example, at orientations $\mathbf{M} \parallel [001]$ and $\mathbf{M} \parallel [110]$ the tensor $\sigma_{\alpha\beta}$ takes in the case of a cubic structure the form (see, e.g., Refs. 11 and 12):

$$\sigma_{\alpha\beta}^{[001]} = \begin{pmatrix} \sigma_{xx} & \sigma_{xy} & 0 \\ -\sigma_{xy} & \sigma_{xx} & 0 \\ 0 & 0 & \sigma_{zz} \end{pmatrix}, \quad \sigma_{\alpha\beta}^{[110]} = \begin{pmatrix} \sigma_{xx} & \sigma_{xy} & \sigma_{xz} \\ \sigma_{xy} & \sigma_{xx} & -\sigma_{xz} \\ -\sigma_{xz} & \sigma_{xz} & \sigma_{zz} \end{pmatrix},$$

i.e., at $\mathbf{M} \parallel [100]$ the off-diagonal components of the tensor have only components odd in \mathbf{M} to describe the MOKE, while for other orientations of \mathbf{M} both odd and even components can be present. To simplify the calculations and their

analysis we have considered the case of only one orientation $\mathbf{M} \parallel [001]$. In this case one can use in the analysis of a numerical calculation of $\sigma_{xy}(\omega)$ for cubic structures an expression obtained by perturbation theory in the SOI and similar to the Argyres equation.¹³

$\text{Im } \sigma_{xy}(\omega) =$

$$\frac{\pi e^2}{\hbar \omega m^2} \sum_{\mathbf{k}, m' \neq m} \{ F_{m'm\uparrow}^{xy}(\mathbf{k}) f_{\mathbf{k}m'\uparrow} (1 - f_{\mathbf{k}m\uparrow}) \delta(\hbar\omega - E_{mm'\uparrow}(\mathbf{k})) - F_{m'm\downarrow}^{xy}(\mathbf{k}) f_{\mathbf{k}m'\downarrow} (1 - f_{\mathbf{k}m\downarrow}) \delta(\hbar\omega - E_{mm'\downarrow}(\mathbf{k})) \}, \quad (1)$$

$$F_{m'm\sigma}^{xy}(\mathbf{k}) = 2i \sum_l \left[\frac{L_{lm'}^{z*}}{E_{ml}} p_x^{lm'} p_y^{mm'} + \frac{L_{lm}^z}{E_{ml}} p_x^{lm'} p_y^{m'm} \right]_{\sigma}$$

where

$$L_{lm\sigma}^z = \langle \mathbf{k} | \hat{l}_z | \mathbf{k} m \sigma \rangle, \quad \xi(r) = \frac{2}{rc^2} \frac{\delta V_{eff}}{\delta r}$$

is the radial SOI parameter, \hat{l} is the angular-momentum operator, $V_{eff}(r)$ is the effective potential of the single-particle Schrödinger equation, and $|\mathbf{k} m \sigma\rangle$ denotes a nonrelativistic state ($\sigma = \uparrow, \downarrow$). Equation (1) is valid only for sufficiently high frequencies $\hbar\omega \gg 2\bar{\xi}/\hbar$ ($2\bar{\xi}$ is the average spin-orbit splitting). At light energies $\hbar\omega \approx 2\bar{\xi}$, an important role in the formation of $\sigma_{\alpha\beta}(\omega)$ is played by hybridization of bands with opposite spins in the vicinity of E_F . The regions of intersection of band sheets with opposite spins ($m\uparrow$) and ($m'\downarrow$) on the Fermi level (line L) yield for $\hbar\omega \approx 2\bar{\xi}$ the following contribution to the conductivity tensor (we present for brevity only the expression for the diagonal component $\text{Re } \sigma_{xx}(\omega)$; for details see Refs. 12 and 14):

$$\text{Re } \sigma_{xx}(\omega) \approx \frac{\pi e^2}{(2\pi)^3 \hbar} \oint_L \frac{d\mathbf{k} |\xi_{\mathbf{k}}|^2 \theta(\hbar\omega - 2|\xi_{\mathbf{k}}|) |\mathbf{p}_x^-(\mathbf{k})|^2}{(\hbar^2 \omega^2 - 4|\xi_{\mathbf{k}}|^2)^{1/2} |[\mathbf{p}^-(\mathbf{k}) \mathbf{x} \mathbf{p}^+(\mathbf{k})]|}, \quad (2)$$

where

$$\mathbf{p}^{\pm}(\mathbf{k}) = \frac{1}{2} [\mathbf{p}_{m\uparrow}(\mathbf{k}) \pm \mathbf{p}_{m'\downarrow}(\mathbf{k})], \quad \xi_{\mathbf{k}} = \langle \mathbf{k} m \uparrow | \hat{\xi} \sigma | \mathbf{k} m' \downarrow \rangle.$$

Evidently allowance for the SOI leads to a characteristic singularity of the conductivity tensor—to a peak at $\hbar\omega \approx 2\bar{\xi}$.

2. CHARACTERISTICS OF ELECTRON SPECTRA

TMnZ compounds with MgAgAs structure have a lower symmetry than the usual Heusler alloys $T_2\text{MnZ}$ from which they are derived. It is indeed the lowering of the symmetry from the total cubic group O_h to the total tetrahedral group T_d which determines mainly the characteristic features of the electron spectrum of the TMnZ compounds.² The absence of inversion in the T_d group makes impossible a hybridization of the antibonding d -orbitals of Mn and p -orbitals of Sb in the compounds NiMnSb and PtMnSb, which leads to the onset of a minimum of the density of the electron states in both spin subbands. Since the p states of Sb are split by exchange interaction much less ($2\Delta_{xc}^p \approx 0.3$ eV) than the d states of Mn ($2\Delta_{xc}^d \approx 3.0$ eV), the magnetic moment is almost completely localized on the Mn atoms,¹⁵ and an effective gap is produced in the SSI and exceeds greatly (by 4–5 times) the analogous gap in the electron SSA. In NiMnSb and PtMnSb compounds the Fermi level turns out to be inside the indicated gap in the SSA, and it is this which determines the wemimetallic ferromagnetism. This is seen from Figs. 1–3, which show the state densities obtained as a result of spin-polarized scalar-relativistic and relativistic (SOI) FTIR calculations carried in (1/6) IPBZ (for TMnZ structures) and (1/16) IPBZ (for the NaCl structure).

In view of the structural and magnetic properties of NiMnSb and PtMnSb (Ref. 16; the lattice parameters are $a_{\text{NiMnSb}} = 5.927$ Å, $a_{\text{PtMnSb}} = 6.195$ Å, and the magnetic moments are $\mu_{\text{NiMnSb}} = 4.2\mu_B$, $\mu_{\text{PtMnSb}} = 3.96\mu_B$), the electron spectra of these compounds have much in common. The Fermi level is located between the d^{\uparrow} and d^{\downarrow} peaks of Mn. The lower part of the valence band is made up of sp states of Sb, the s^{\downarrow} states of Sb are located in the vicinity of E_F , and the s^{\uparrow} states of Sb form peaks above E_F (the s^{\downarrow} states of Sb become strongly hybridized with the d^{\downarrow} states of Mn). The central part of the valence band (below E_F) are made up of Ni (Pt) d states hybridized with the p states of Sb and the d^{\downarrow} states of Mn. The main changes produced in the spectrum when Ni is replaced by Pt are due to SOI effects, which are considerably larger in Pt ($2\bar{\xi} \approx 0.5$ eV) than in Ni ($2\bar{\xi} \approx 0.18$ eV). As seen from a comparison of Figs. 2 and 3, the SOI effects lead to an effective broadening and smoothing of the density of the d states of Pt because of the almost complete lifting of the degeneracy due to the symmetry of the crystal (if the point group T_d is of order 24, the order of the magnet-

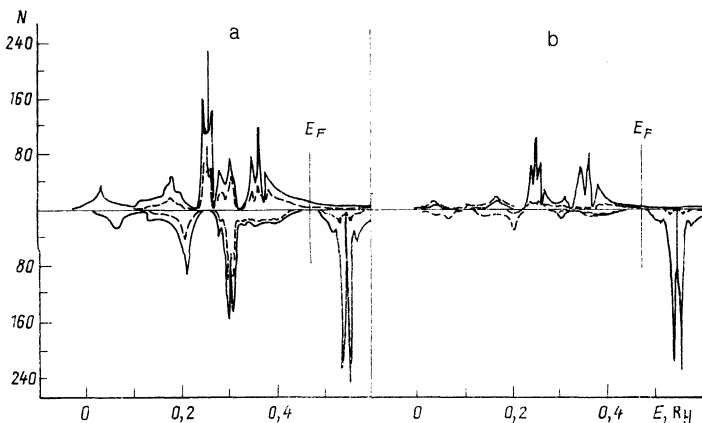


FIG. 1. State densities $N(E)$ (st./Ry·el·nucl. spin units) in NiMnSb without allowance for SOI: a) solid curve—total density of states, dashed— d -state density in Ni; b) solid curve— s -state density in Mn, dashed— p -state density in Sb.

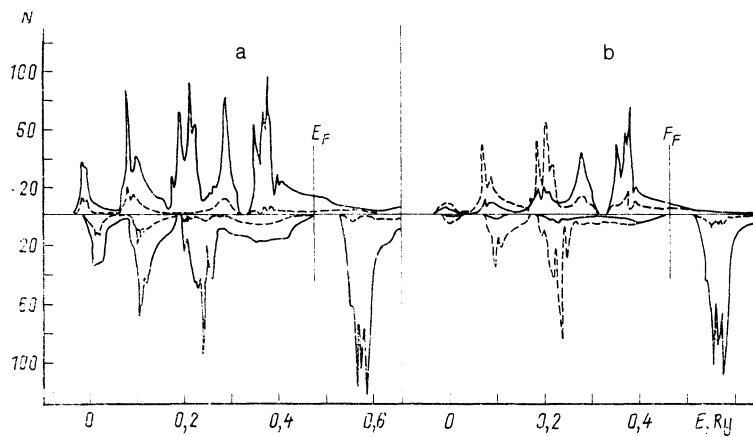


FIG. 2. The same as in Fig. 1, for PtMnSb: a) solid curve—total density of states, dashed— p -state density of Sb; b) solid curve—total d -state density of Mn, dashed— d -state density of Pt.

ic-crystal class at $\mathbf{M} \parallel [001]$ is 8).

If SOI effects are omitted from the band calculations, the NiUSn spectrum has, as seen from Fig. 4, much in common with the NiMnSb spectrum. The vicinity of E_F is now made up of $5f$ states of U, but the SSI has a gap where E_F passes, just as in the NiMnSb case. This gap, as in Ni(Pt)MnSb, is due to the absence from the point group of inversion that causes mutual repulsion of the p states of Sn and the f states of U. Allowance for SOI, as seen from Fig. 5, leads to a considerable broadening (from 1.2 to 2.5 eV) and to a smoothing of the density of the f states of U (which decreases by 2–3 times), in agreement with experiment,¹⁷ attributed to the appreciable spin-orbit splitting ($2\bar{\xi} \approx 1.5$ eV). On the other hand, the splitting of the f states by the SOI decreases effectively the gap in the SSI, so that on the Fermi level the density of states turns out to differ from zero not only for the SSA but also for the SSI of the electrons (in view of the strong LS coupling this will occur more accurately if the states are characterized by the projection of the total angular momentum $\hat{j} = \hat{l} + \hat{s}$, i.e., $j_{\pm} = l \pm 1/2$). It appears thus that NiUSn can hardly be classified as an HMF as stated earlier.³ Inclusion of the SOI in the calculation also alters substantially the magnetic moment ($2.0\mu_B$ and $2.6\mu_B$ without and with allowance for the SOI), which is practically entirely localized on U.

In another uranium-containing compound, the monochalcogenide US, the magnetism and conductivity are also due to $5f$ states of U. Since this compound corresponds to the higher-symmetry group O_h , while the p states of S and

the f states of U are greatly separated in energy (by 2.5 eV), the gap responsible for the SMF is not produced here. Inasmuch, however, as the spin-orbit and exchange splittings of the f states are of the same order ($2\bar{\xi} \approx 2\Delta_{xc}^f \approx 1.5$ eV), a gap of order $2\bar{\xi}$, due to the SOI, is produced in the two states $j = l + 1/2$ and $f = l - 1/2$ (Fig. 6). Thus, the entire f band breaks up into two subbands with an interval $\approx 2\bar{\xi}$ between them, and with E_F passing the lower one. Strong changes of the kinetic properties should be expected, depending on the type of doping.

3. OPTICAL AND MAGNETOOPTIC PROPERTIES

NiMnSb

Calculated and experimental¹⁸ results for the interband part of the diagonal component $\text{Re } \sigma_{xx}(\omega)$ of the conductivity tensor are shown in Fig. 7. It is known that if SOI effects are not taken into account the optical conductivity is a sum of components, $(\text{Re } \sigma_{xx}^i)$ and $(\text{Re } \sigma_{xx}^{\text{int}})$, describing the contributions from the interband transitions to the SSA and the SSI, respectively (Fig. 7). This subdivision is convenient not only for the interpretation of the optical-conductivity singularities, but also, as shown in Ref. 1, for the understanding of the dependence of off-diagonal component $\text{Im } \sigma_{xy}(\omega)$ of the conductivity tensor. Noteworthy among the principal singularities of $\text{Re } \sigma_{xx}(\omega)$ in NiMnSb is the presence a threshold at $\hbar\omega \leq 0.6$ eV for interband transitions and of a large maximum at $\hbar\omega \approx 3.4$ eV. The former singularity is due to the presence of a gap in the SSI and to the the low

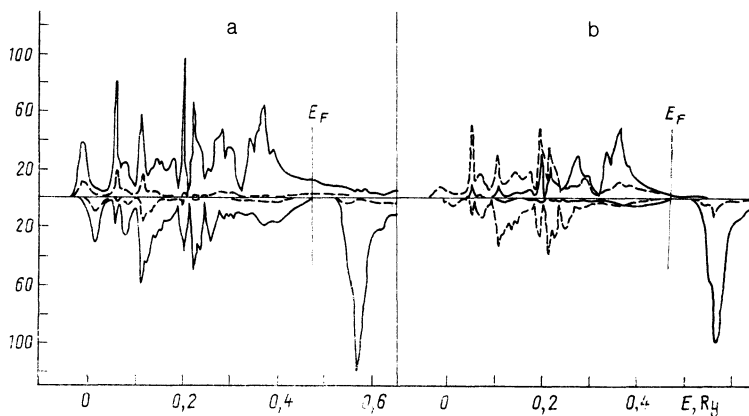


FIG. 3. The same as in Fig. 2, but with SOI taken into account.

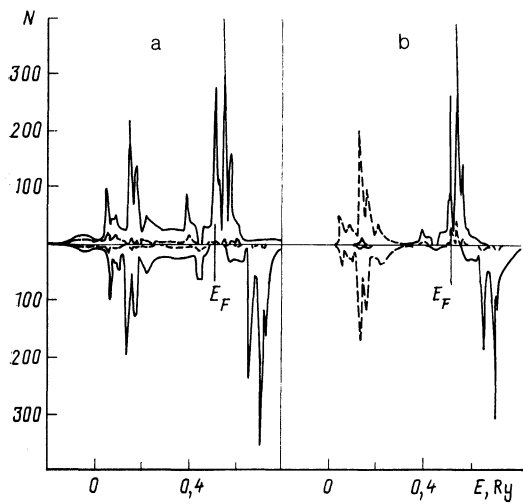


FIG. 4. The same as in Fig. 1 but of NiUSn: a) solid curve—total density, dashed— p -state density of Sn; b) Solid curve— f -state density of U, dashed— d -state density of Ni.

density of states of the SSA in the vicinity of E_F .

The nonzero $\text{Re } \sigma_{xx}(\omega)$ at $\hbar\omega \approx 0.7$ eV is due to transitions between $(pd)^{\uparrow}$ -hybridized states of Sb and Ni in the vicinity of the Γ -centered hole spheres. The wide peak in the region $\hbar\omega \approx 3.4$ eV is due to $p_{\text{Sb}}^{\downarrow} \rightarrow d_{\text{Mn}}^{\downarrow}$ transitions in the SSI (see Fig. 7b)

As seen from Fig. 8, the main singularities of the component $\text{Im } \sigma_{xy}(\omega)$, which are of interest from the standpoint of a large MOKE, lie in the energy interval $\hbar\omega \approx 1.6 - 2.9$ eV. The origin of the singularities is easiest to understand by turning to the Argyres formula (1). According to (1), dipole transitions, in magnetooptics, are effected in first-order perturbation theory between fixed bands m and m' through "intermediate" bands l via SOI, and the SOI matrix elements $L_{lm\sigma}^z$ are diagonal in the spin and in the orbital momentum. As seen from (1), $\text{Im } \sigma_{xy}(\omega)$ has at $\hbar\omega \gg 2\bar{\xi}$ two components, one with spin up and the other with spin down, and both components have [disregarding the structure of the

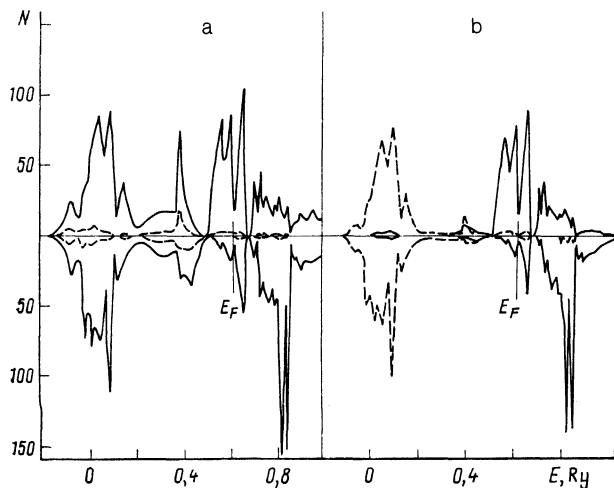


FIG. 5. The same as in Fig. 4, but with allowance for SOI.

matrix elements $F_{m'm\sigma}^{xy}(\mathbf{k})$ of the transitions] the structure of the diagonal components of $\text{Re } \sigma_{xx}(\omega)$.

From the foregoing, as well as from the analysis of the band structure, it follows that at $0.6 \text{ eV} \leq \hbar\omega \leq 2.0 \text{ eV}$ we have $\text{Im } \sigma_{xy}(\omega) \approx \text{Re } \sigma_{xx}^{\downarrow}(\omega)$, as is in fact seen from Fig. 7b. In particular, at the energy $\hbar\omega \approx 2.0$ eV (at which, according to numerical estimates, the maximum MOKE takes place), $\text{Im } \sigma_{xy}(\omega)$ is the result of transitions in the central part of the Brillouin zone between hybridized d^{\downarrow} states of Ni and Mn and p^{\downarrow} states of Sb via the indicated d^{\downarrow} states. At energies $2.0 \text{ eV} < \hbar\omega < 3.0 \text{ eV}$ we have $\text{Im } \sigma_{xy}(\omega) \approx \text{Re } \sigma_{xx}^{\uparrow}(\omega)$ (see Fig. 7b), i.e., they are formed mainly via $p_{\text{Sb}}^{\downarrow} \rightarrow d_{\text{Mn}}^{\downarrow}$ transitions to the SSI through the d^{\downarrow} states of Ni and Mn. Thus, in accordance with Eq. (1), the main factors that determine $\text{Im } \sigma_{xy}(\omega)$ (among others such as the exchange splitting, the densities of the states m', m, l , etc.) are: a) the SOI parameter (the numerator in $F_{m'm\sigma}^{xy}$) for hybridized d states of Ni and Mn, through which the transitions are effected, is $2\bar{\xi}_{\text{Ni}} \approx 2\bar{\xi}_{\text{Mn}} \approx 0.15$ eV; b) the "proximity" of the intermediate states l to the states m and m' between which the transitions are effected (denominators in $F_{m'm\sigma}^{xy}$), i.e., if we put $m = d_{\text{Ni,Mn}}^{\downarrow}$, $m' = p_{\text{Sb}}^{\downarrow}$, $l = d_{\text{Ni,Mn}}^{\downarrow} \neq m$ for $\hbar\omega \approx 2.0$ eV, then $(1/E_{ml\uparrow}) \approx 1-2 \text{ eV}^{-1}$ (the factor $L_{lm\sigma}^z/E_{m'l} \approx 0$). It should be noted that although the positions of the calculated and experimental ($\hbar\omega \approx 1.5$ eV, Ref. 1) MOKE maxima are quite close, the calculated value of the Kerr angle is several times larger than the experimental value. A possible explanation is failure to take the relaxation of the electron states into account.

PtMnSb

Replacement of Ni by Pt does not lead to noticeable changes of $\text{Re } \sigma_{xx}(\omega)$ (Fig. 9a), as expected from the identity of the electron spectra of NiMnSb and PtMnSb. The off-diagonal components, however, undergo more significant change, owing to the considerably larger SOI parameter, $2\bar{\xi}_{\text{Pt}} \approx 0.5$ eV. Since remaining factors for NiMnSb and PtMnSb are quite close, one should expect for PtMnSb an enhancement of $\text{Im } \sigma_{xy}(\omega)$ by $2\bar{\xi}_{\text{Pt}}/2\bar{\xi}_{\text{Ni}} \approx 3$ times. To be sure, this effect is decreased somewhat by broadening and by the decrease of the density of the d states of Pt via the SOI that lifts the degeneracy of the spectrum. The calculated $\text{Im } \sigma_{xy}(\omega)$ curves for PtMnSb (Fig. 9b) and NiMnSb have on the whole much in common, although on the average the amplitude of $\text{Im } \sigma_{xy}$ in the case of PtMnSb is approximately 2.5 times larger than that of NiMnSb. Estimates of the Kerr angle show that the MOKE is a maximum in the vicinity of $\hbar\omega \approx 2.5$ eV, which is much higher than the experimental value of the position of MOKE maximum at $\hbar\omega \approx 1.7$ eV.¹ This discrepancy is possibly due to the strong dependence of the Fermi level on the form of the exchange-correlation potential used in the band calculations.⁴ It should also be noted that although the calculated value of the maximum Kerr angle is of the same order as in experiment, Replacement of Ni by Pt does not increase the MOKE as sharply in the calculations as in experiment.¹

We can mention in this connection a number of studies of this problem.^{5,19} It is stated in the recent Ref. 19 that the difference between the magneto optic properties of NiMnSb and PtMnSb is due primarily to scalar-relativistic effects and to SOI effects. The analysis above, however, shows that one

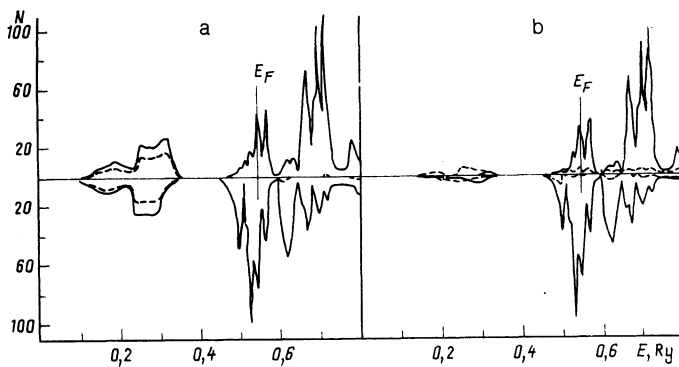


FIG. 6. The same as in Fig. 1, but for US: a) solid curve—total S-state density, dashed—*p*-state density of S; b) solid curve—*f*-state density of U, dashed—*d*-state density of U.

can hardly neglect the SOI difference between these crystals, since the MOKE is the result of SOI not with Sb, as proposed in Ref. 19, but with Ni and Pt. It is quite possible that the discrepancy between theory and experiment is due, on the one hand, to the use in the calculations of a local approximation for the exchange-correlation potential, and on the other to the insufficient accuracy of the determination of the dispersive components of the conductivity tensor in the estimate of the Kerr angle. These questions are being thoroughly investigated at present.

NiUSn

One might expect that replacement of Mn in PtMnSb by a 5*f* element would enhance the MOKE on account of the sharp increase of the SI, $2\xi_U \approx 1.5$ eV. The magnetic mo-

ment $\mu_{\text{NiUSn}} = 2.0\mu_B$, however, turns out to be half as large as in PtMnSb. As a result the maximum of $\text{Im } \sigma_{xy}(\omega)$ is approximately of the same order as as in PtMnSb (Fig. 10b). Moreover, NiUSn absorbs light more strongly than PtMnSb, i.e., $[\text{Re } \sigma_{xx}(\omega)]_{\text{NiUSn}} > [\text{Re } \sigma_{xx}(\omega)]_{\text{PtMnSb}}$ (Fig. 10a). Since, roughly speaking, the MOKE is determined by the ratio of the off-diagonal and diagonal components,²⁰ the maximum Kerr angle for NiUSn turns out to be smaller than for PtMnSb, although a considerably larger effect was previously predicted.⁶

Let us discuss briefly the cause of the singularities of the tensor. The broad peak of $\text{Re } \sigma_{xy}(\omega)$ at $4.2 \text{ eV} < \hbar\omega < 4.8 \text{ eV}$ is due to transitions $d_{\text{Ni}}^{\uparrow} \rightarrow f_{\text{U}}^{\uparrow}$ and $d_{\text{Ni}}^{\downarrow} \rightarrow f_{\text{U}}^{\downarrow}$ in both the SSI and SSA of the electrons and, just as at other frequencies, the transitions in the SSA are comparable by virtue of the relatively small value of the exchange splitting ($2\Delta_{xc}^f \approx 1.4$ eV), with the transitions in the SSI [the difference $\text{Re } \sigma_{xx}^{\uparrow}(\omega) - \text{Re } \sigma_{xx}^{\downarrow}(\omega)$, according to (1), is just the measure of $\text{Im } \sigma_{xy}(\omega)$]. The peak of $\text{Im } \sigma_{xy}(\omega)$ at $\hbar\omega \approx 1.2$ eV is due to transitions, in the SSA, between the hybridized (*pd*)[↑] states of Ni, U, and Sn, and the *f*[↑] states of U. There are practically no transitions in the SSI because of the low density of states in the vicinity of E_F at $\hbar\omega < 1.5$ eV. At $\hbar\omega \approx 2.1$ eV, however, the (*pd*)[↓]_{Ni,U,Sn} $\rightarrow f_{\text{U}}^{\downarrow}$ transitions that arise in the SSI (via the quasigap) lead to the onset of a peak of $\text{Im } \sigma_{xy}(\omega)$. The calculated Kerr angle is a maximum at $\hbar\omega \approx 1.2$ eV.

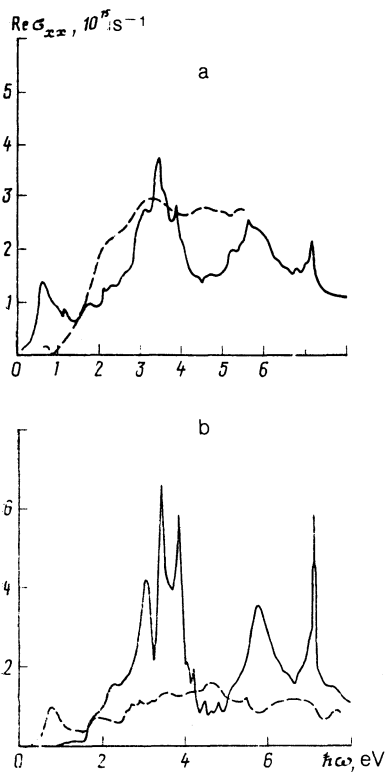


FIG. 7. Dissipative part of the diagonal component of the conductivity density $\text{Re } \sigma_{xx}(\omega)$ for NiMnSb: a)—solid curve—total conductivity, dashed—experiment; b) partial spin contributions $\text{Re } \sigma_{xx}^{\uparrow}(\omega)$ (dashed) and $\text{Re } \sigma_{xx}^{\downarrow}(\omega)$ (solid curve).

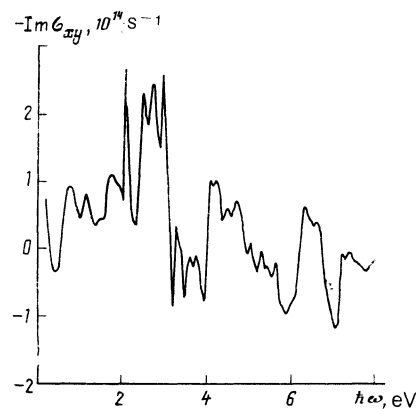


FIG. 8. Dissipative part of off-diagonal component of the conductivity tensor $\text{Im } \sigma_{xy}(\omega)$ for NiMnSb.

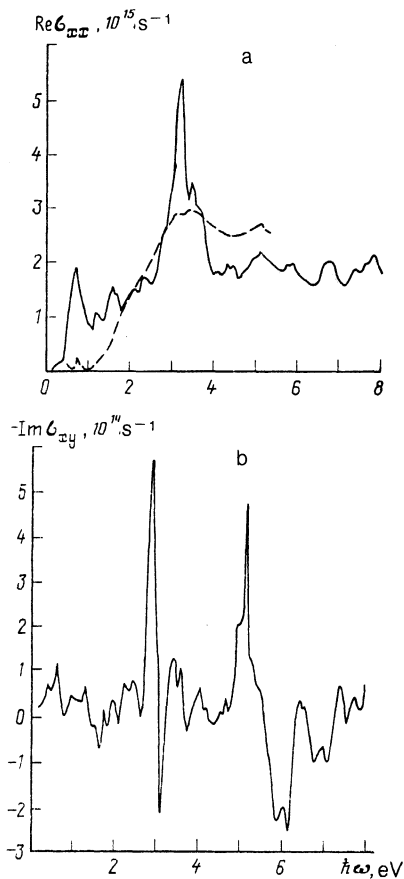


FIG. 9. The same as in Fig. 7a, for PtMnSb; b) the same as in Fig. 8, for PtMnSb.

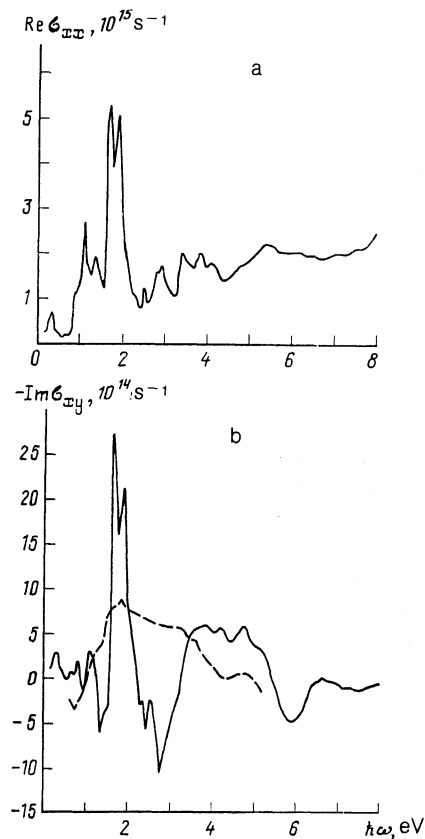


FIG. 11. The same as Fig. 10 (the solid curve in Fig. b is calculated, the dashed is experimental²³).

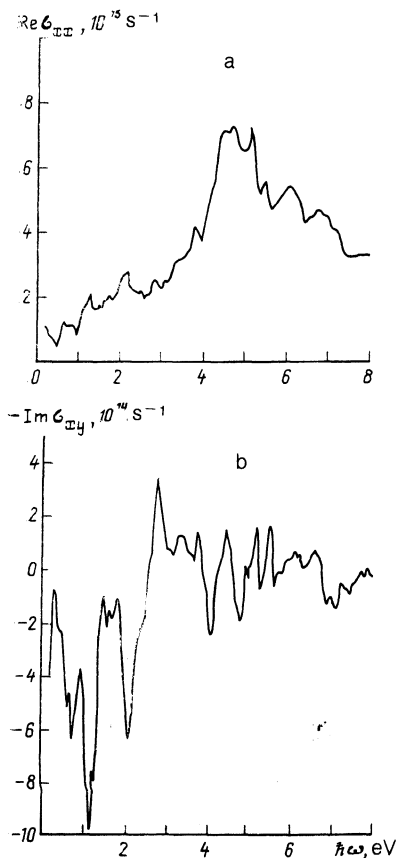


FIG. 10. Optical characteristics of NiUSn: a) interband part of diagonal component of the conductivity tensor $\text{Re } \sigma_{xx}(\omega)$. b) imaginary part of off-diagonal component of the conductivity tensor $\text{Im } \sigma_{xy}(\omega)$.

It became recently known^{21,22} that, unfortunately, no ferromagnetic phase of NiUSn has been produced in experiment: what is realized in fact in the ground state is an antiferromagnetic phase (FCC, type I) with a magnetic moment $(1.42 \pm 0.03) \mu_B$ parallel (antiparallel) to the [100] cubic axis on the U atom. The Néel temperatures ($T_N = 47$ K and 43 K in Refs. 21 and 22, respectively) separate a paramagnetic semiconducting (!) phase from an antiferromagnetic metallic phase. The foregoing analysis of the electron spectrum and optical properties of the ferromagnetic phase (obviously unstable and realized only by action of a strong magnetic field) of NiUSn permits us, nevertheless to predict an appreciable MOKE in such isostructural ferromagnets as CoUSn and PdUSn.

US

In US compounds, where the SOI and exchange-splitting parameters are of the same order ($2\xi_U \approx 2\Delta_{xc}^f \approx 1.5$ eV), strong hybridization (on account of the SOI) of bands with opposite spin projections leads in the vicinity of E_F to a new conductivity-tensor formation mechanism. As indicated in Sec. 1, interband transitions resulting from hybridization by the SOI with simultaneous participation of the SSI and SSA of the electrons lead to the onset of $\text{Re } \sigma_{xx}(\omega)$ and $\text{Im } \sigma_{xy}(\omega)$ peaks at an energy $\hbar\omega \approx 2\xi_U$. In Fig. 11, $\text{Re } \sigma_{xx}(\omega)$ and $\text{Im } \sigma_{xy}(\omega)$ have sharp peaks at $\hbar\omega \approx 1.6$ eV, in full agreement with Eq. (2) [see also Eq. (17) of Ref. 12]. These singularities are due to $d \rightarrow f$ transitions in the U atom.

The second sharp peak of $\text{Im } \sigma_{xy}(\omega)$ is due to transition between hybridized (pd) and (df) states of S and U. Calculated

lations yield a maximum Kerr angle at $\hbar\omega \approx 1.6$ eV because of the indicated SOI effect, in good agreement with experiment,²³ although the calculated value is several times larger than the experimental. At 4.4 eV a noticeable enhancement of the MOKE takes place both in the calculations and in experiment.

CONCLUSION

As shown by numerical calculations and by their analysis, 100% spin correlation on the Fermi level (i.e., the presence of a gap in the minority spin band of the electrons) and large values of the SOI do not by themselves guarantee a large MOKE. Numerical investigations of the electron spectrum and of the optical properties of NiMnSb and PtMnSb have revealed in the latter an increase, due to the different values of the SOI at the Ni and Pt atoms, of the amplitude of the off-diagonal components of the conductivity tensor. At the same time, the MOKE amplitude is determined, besides by the SOI, by specific features of the electron spectrum and by the presence of plasma resonance. An illustrative idea of the role played by the semiconductor gap in the formation of the MOKE can be obtained by comparing the electronic and optical properties of NiUSn and US, with US not a semimetallic ferromagnet. Just the last circumstance, i.e., the absence of a gap in both spin-subbands, and hence the presence of intersection of nonrelativistic bands with opposite spins, is the condition for realization of the interband mechanism that leads to the strong enhancement of the MOKE in US at frequencies of the order of the SOI (in U).

The authors hope that this analysis of the investigated compounds will be useful for the understanding of the electronic, optical, and magneto-optic properties of a new class of substances—semimetallic ferromagnets.

The authors thank V. G. Veselago, E. G. Maksimov,

Yu. A. Uspenskii, and I. I. Mazin for interest in the work and for helpful discussions of the calculation results.

- ¹ P. G. van Engen, K. H. J. Buschow, R. Jongenbreur, and M. Erman, *Appl. Phys. Lett.* **42**, 202 (1983).
- ² R. A. de Groot, F. M. Mueller, P. G. van Engen, and K. H. J. Buschow, *Phys. Rev. Lett.* **50**, 2024 (1983).
- ³ R. C. Albers, A. M. Boring, G. H. O. Daalderop, and F. M. Mueller, *Phys. Rev. B* **36**, 3661 (1987).
- ⁴ E. Kulatov and I. I. Mazin, *J. Phys.: Condens. Mat.* **2**, 343 (1990).
- ⁵ H. Feil and C. Haas, *Phys. Rev. Lett.* **58**, 65 (1987).
- ⁶ G. H. O. Daalderop, F. M. Mueller, R. C. Albers, and A. M. Boring, *Appl. Phys. Lett.* **52**, 1636 (1988).
- ⁷ O. K. Andersen, *Phys. Rev. B* **12**, 3060 (1975).
- ⁸ C. C. Itzykson and J.-B. Zuber, *Quantum Field Theory*, McGraw, 1980.
- ⁹ R. Kubo, *J. Phys. Soc. Japan* **12**, 570 (1957).
- ¹⁰ Yu. A. Uspenskii, E. G. Maksimov, I. I. Mazin, and S. N. Rashkeev, *Z. Physik B* **53**, 263 (1983).
- ¹¹ W. H. Kleiner, *Phys. Rev.* **142**, 318 (1966).
- ¹² Yu. A. Uspenskii and S. V. Khalilov, *Zh. Eksp. Teor. Fiz.* **95**, 1022 (1989) [*Sov. Phys. JETP* **68**, 588 (1989)].
- ¹³ P. N. Argyres, *Phys. Rev.* **97**, 334 (1955).
- ¹⁴ S. V. Khalilov and Yu. A. Uspenskii, *Fiz. Met. Metallov.* **66**, 1097 (1988).
- ¹⁵ J. Kuebler, A. R. Williams, and C. B. Sommers, *Phys. Rev. B* **28**, 1745 (1983).
- ¹⁶ M. J. H. Otto, R. A. M. van Woerden, P. J. van der Valk *et al.*, *J. Phys.: Condens. Mat.*, **1**, 2341 (1989).
- ¹⁷ H. Hoehst, K. Tan, K. H. J. Buschow, *J. Magn. Magn. Mat.* **54–57**, 545 (1986).
- ¹⁸ P. A. van der Heide, W. Baelde, R. A. de Groot *et al.*, *J. Phys. F* **15**, L75 (1985).
- ¹⁹ J. H. Wijnngaard, C. Haas, and R. A. de Groot, *Phys. Rev. B* **40**, 9317 (1989).
- ²⁰ H. S. Bennett and E. A. Stern, *Phys. Rev.* **136**, A448 (1965).
- ²¹ M. Yethiraj, R. A. Robinson, J. J. Rhyne *et al.*, *J. Magn. Magn. Mat.* **79**, 355 (1989).
- ²² K. Kojima, Y. Hukuda, H. Kawanaka *et al.*, *Yamada Conf. XXV on Magnetic Phase Transitions, Abstracts and Program, Osaka, Japan, April 13–16 (1990)*, p. 143. Y. Aoki, T. Suzuki *et al.*, *ibid.* p. 143.
- ²³ W. Reim, *J. Magn. Magn. Mat.* **58**, 1 (1986).

Translated by J. G. Adashko